Using Hybrid Energy Storage System for Grid-Connected Photovoltaic Applications

Ghadder Ghabour[1], Mohamad Amir Hababa[1], Waseem Saeed[1] and Muzaffar Murodov[2]
[1]*Electrical Energy Engineering, Damascus University, 11141 Damascus, Syria*
[2]*Department of Power Engineering, Namangan State Technical University, I. Karimov Str. 12, 160100 Namangan, Uzbekistan*
ghadder.ghabour@damascusuniversity.edu.sy, amir.hababa@damascusuniversity.edu.sy, waseem.saeed@damascusuniversity.edu.sy, m_murodov@mail.ru

Keywords: Modelling, Supercapacitors, The Maximum Power Point Tracking MPPT, Bidirectional DC-DC Converters (BDC) Buck/Boost, PI Controller, Energy Density, Power Density.

Abstract: This paper presents the design and modeling of a hybrid energy storage system (HESS) for a grid-connected photovoltaic (PV) application. The proposed system integrates batteries and supercapacitors to address the inherent variability of solar power generation and to enhance grid stability. A boost converter is employed to regulate and elevate the PV output voltage, while a maximum power point tracking (MPPT) algorithm based on the incremental conductance method ensures optimal energy extraction under varying environmental conditions. The system is interfaced with the grid through a three-phase voltage source inverter controlled by pulse width modulation (PWM). The hybrid storage configuration combines the high energy density of batteries with the high power density of supercapacitors, enabling efficient management of both low-frequency and transient power fluctuations. A bidirectional DC–DC buck–boost converter with PI-based control is used to coordinate charging and discharging processes. Simulation results demonstrate that the proposed system effectively reduces power fluctuations, minimizes grid dependency during peak demand, and improves overall system reliability. Furthermore, the hybrid approach alleviates battery stress, thereby extending its operational lifetime. The study confirms that integrating hybrid energy storage significantly enhances the performance and stability of grid-connected PV systems.

1 INTRODUCTION

The power generation from renewable energy sources is inherently variable due to their dependence on fluctuating weather conditions. For instance, the energy output from recently deployed photovoltaic systems is highly variable [1], [2]. These energy fluctuations pose challenges to the stability of the public grid and the overall power system. Therefore, the use of energy storage systems can mitigate these instability issues. Since the inception of electrical energy generation, various effective technologies have been developed to store and utilize energy when demand arises. The energy storage industry has continued to evolve and advance technically, diversifying both the technologies and the methods for controlling power sources. This diversification aims to create a flexible energy infrastructure and achieve cost savings for both network owners and consumers. Batteries have been utilized as a crucial storage element, with research identifying the optimal size to minimize total operating costs [1]. Additionally, other energy storage systems, such as supercapacitors, have been employed to address the variability in the output power of distributed photovoltaic systems injected into the grid, demonstrating their impact on the safety and reliability of distribution networks [2]. Figure 1 illustrates the energy density and power density of each storage type, thereby determining the optimal operating range for each.

The concept of power density, which represents the maximum power that can be extracted per unit mass (W/kg), and the concept of energy density, which denotes the energy that can be expended from the source per unit mass (Wh/kg), are pivotal in the realm of energy storage. These concepts determine the optimal energy source based on the application. For instance, for long-term operation, sources with high energy density, such as certain storage

technologies with high energy density, are preferred to extend the operating time of the load. Conversely, when a large capacity is required irrespective of time, supercapacitors with high power density (KW/kg) are more suitable, making them ideal for applications like engine starting or braking [3], [13]. Consequently, it has been found that the advantages of both storage elements can be harnessed through a hybrid storage system. This system comprises as Figure 2.

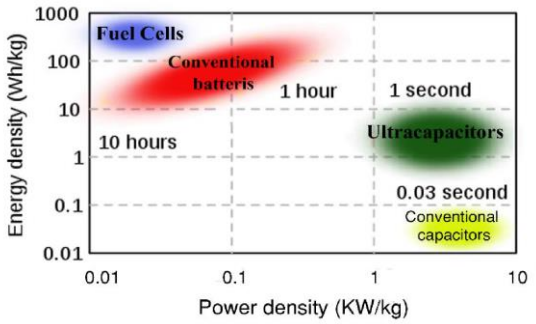

Figure 1: Energy density and power density of supercapacitors and Batteries [3], [13].

Energy Storage unit (ESU1): Designed to meet high power demand and rapid, transient load changes, characterized by fast response time, high efficiency, and long-life cycle.

Energy Storage unit (ESU2): Intended for high energy storage, characterized by a low self-discharge rate and low energy installation cost [4], [14], [28].

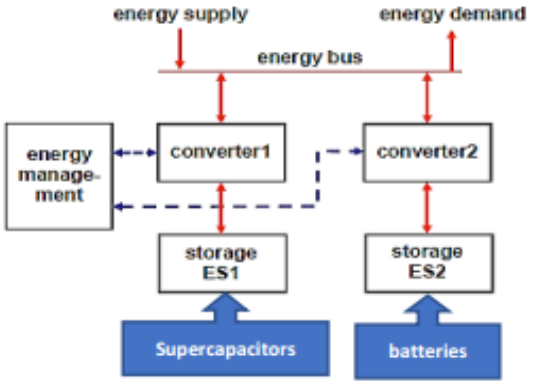

Figure 2: Basic structure of hybrid storage system.

The two storage units are charged and discharged using a bidirectional DC/DC converter. Borkowski ,D. Oramus ,P & Brzezinka ,M In [1], a dedicated control strategy for PV-BESS that maximizes the daily market DM revenue is proposed. The algorithm for determining the control strategy was implemented using analytical methods based on complete data on PV production and energy prices. Furthermore, the control strategy was implemented in a sizing algorithm that optimized the financial criteria. The effectiveness of the algorithm was demonstrated through an example of real 1 MW PV data. A 10-year analysis of the system operation using the additional control mode indicated a significant increase in the rate of return of the energy storage, reaching 15 % for the high PV penetration price profile. Gonçalves, A. Cavalcanti, G & Feitosa, M&..etc In [2] the size of the BESS system was determined to supply energy to the load of auxiliary systems of an ESS, as well as a PV system to achieve a null total cost. Furthermore, multi-objective optimization using the genetic algorithm technique was employed to optimize the size of the hybrid PV/BESS to minimize the investment cost and time when the demand was not met. Simulations under different scenarios of contingency were allowed to obtain the Pareto frontier for the optimal sizing of a PV/BESS system to supply energy to AC auxiliary systems in an ESS under contingency. Member, S., & Ongaro, F [3].at the University of Udine, Italy, this study focused on extending the lifespan of batteries powering wireless sensors. A DC-DC converter was used to control input voltage and increase power, while a statistical method based on recorded energy data determined the energy storage elements' size. Results showed a significant reduction in charge/discharge cycles of Li-ion batteries, improving their lifespan and confirming the design procedure's validity. Karshenas, Kurtoğlu1, M,&Eroğl, F. In [4] a non-isolated BDC, has a buck and boost principle of operation, is designed, analysed and simulated under various case studies. In the designed system, BDC controls the bidirectional power flow between the battery and DC link. Specifically, in the charging stage of battery operating in buck mode, DC-link supplies the power to the battery and BDC regulates the battery current using proportional-integral (PI) controller. On the other hand, in the discharging stage of the battery operating in boost mode, when DC source is disconnected, the battery supplies the power to DC load and DC-link voltage is controlled by the BDC via PI controller. The simulation results are presented to show the operation and control of the BDC under different scenarios. Manuel, V., & Guerrero, M.Á [5] This research presented a 30 KW photovoltaic system connected to the grid, aiming to develop a method for calculating energy storage system size using energy curves and fuzzy control methods. As for Rajasekaran, R., & Rani, P.U [6] this study employed an energy management algorithm for a standalone

(PV + wind) system to achieve microgrid self-sufficiency. In [7] discusses the transition to renewable energy systems and the challenges of energy storage within them. It addresses the issues of optimizing the capacity of hybrid energy storage systems and their environmental impact. The study presents new strategies to enhance the utilization of these systems and reduce greenhouse gas emissions. Saritha.K.& Sharma.S & another [8] discusses green energy storage technologies, which are a key element in reducing carbon emissions and integrating renewable energy sources. It examines the use of Energy Storage Systems (ESS) to store surplus electricity and make it available on demand to reduce fluctuations. The study reviews green energy storage systems and presents new strategies to enhance their utilization and reduce greenhouse gas emissions.

The current work aims to design and model a hybrid storage system of batteries and supercapacitors for a photovoltaic system that can be connected to the grid. This system can connect regardless of source voltage changes and works to elevate and regulate the output voltage of the photovoltaic system using a boost converter, to operate at the maximum power point of the cells' output. The output voltage then feeds a three-phase voltage inverter driven by PWM (Pulse Width Modulation) technology. When the output power of the photovoltaic system decreases, the stored energy in the batteries and supercapacitors can be utilized, as illustrated in Figure 3.

Based on this study, a hybrid storage system comprising batteries and supercapacitors, along with the necessary bidirectional DC/DC converter (buck-boost) for charging and discharging, was adopted in this research.

2 SYSTEM CONSTRUCTION

The subsequent sections will outline the design equations necessary for a grid-connected photovoltaic system is depicted in Figure 4 (PV system, Boost Converter, Three-phase inverter, Passive filters and grid). as well as the equations required for designing the hybrid storage system and its control components. Additionally, the computer model used to evaluate the overall system performance will be presented.

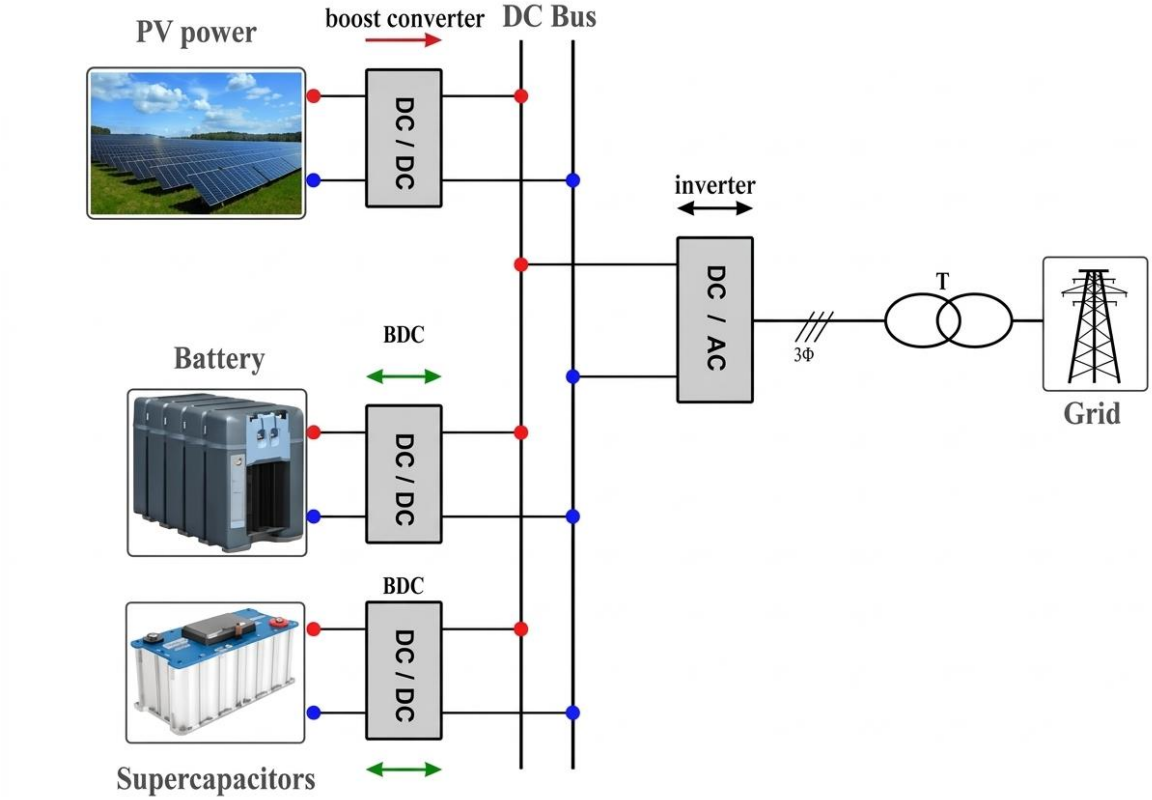

Figure 3: Basic components of the system [9].

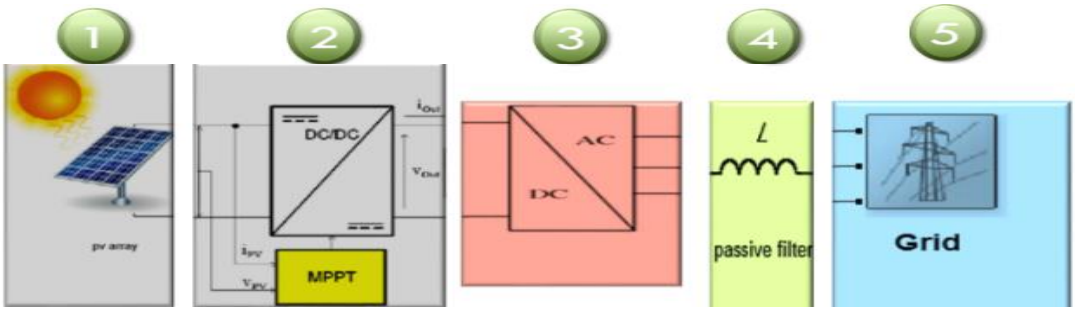

Figure 4: Steps for designing and modeling a grid-connected photovoltaic system.

2.1 PV System

The photovoltaic system array consists of multiple strings connected in parallel, where the total number of modules is calculated using the following relationship:

$$N_{modul} = \frac{P}{P_m}. \quad (1)$$

- P: PV system power [W], P_m: PV module power [W].

The number of modules in a string is calculated as follow

$$N_{m,string} = \frac{V}{V_m}. \quad (2)$$

- V: PV system voltage [V], V_m: PV module voltage [V]

The number of strings connected in parallel is given by:

$$S_p = \frac{N\_modul}{N\_(m,string)}. \quad (3)$$

To design a photovoltaic array with a capacity of 10 [kW] and maximum output voltage of 200 [V] and select a module with a capacity of 630 [W] and maximum output voltage of 46.02[V], the components of the array are determined based on the relationships above (1), (2) and (3):

$$N_{modul} = 16\ ,\ N_{m,string} = 4\ ,\ S_p = 4.$$

2.2 Boost Converter

The boost converter functions to elevate the output voltage of the PV array, as illustrated in Figure 5.

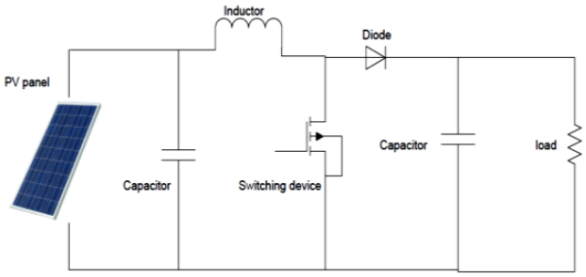

Figure 5: Components of the Boost Converter [10].

The duty factor D, inductor L and capacitor C of converter is calculated according to [15]:

$$D = 1 - \frac{V_i}{V_o},\ L = \frac{(1-D)^2 \times D \times R}{2F},\ C = \frac{D \times V_o}{R \times F \times \Delta V_O}. \quad (4)$$

- V_I: converter input voltage [V];
- V_o: converter output voltage [V];
- R: output resistance [Ω];
- F: chopping frequency [HZ];
- ΔV_O: output voltage ripple [%].

In order to design a boost converter, its input voltage is equal to the output voltage photovoltaic array, 200[V], and its output voltage is 400[V] with ΔV_O<1%, R =500 [Ω], F =50000[HZ] assumed.

Using (4) the nominal values of the elements are determined:

D= 0.5, L= 625*10-6 [H], C = 888*10-6 [F]

2.3 Maximum Power Point Tracking (MPPT)

The incremental conductance method has been selected due to its effectiveness in handling significant variations in weather conditions [16]. This method depends on the values of the slope of the (P-V) curve as in Figure 6.

At the maximum power point:

$$\frac{dI_{PV}}{dV_{PV}} = -\frac{I_{PV}}{V_{PV}}.$$

To the left of the maximum power point:

$$\frac{dI_{PV}}{dV_{PV}} > -\frac{I_{PV}}{V_{PV}}.$$

To the right of the maximum power point:

$$\frac{dI_{PV}}{dV_{PV}} < -\frac{I_{PV}}{V_{PV}}.$$

Therefore, the flow chart for this method is as shown in Figure 7. Figure 8 shows modeling of this method in Matlab.

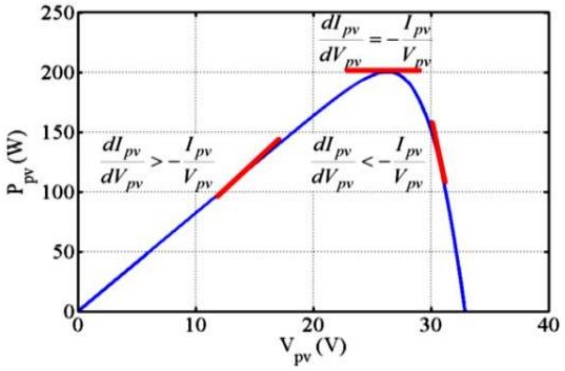

Figure 6: Illustrates the method of increasing conductivity by inclining (power-voltage) curve [10], [16].

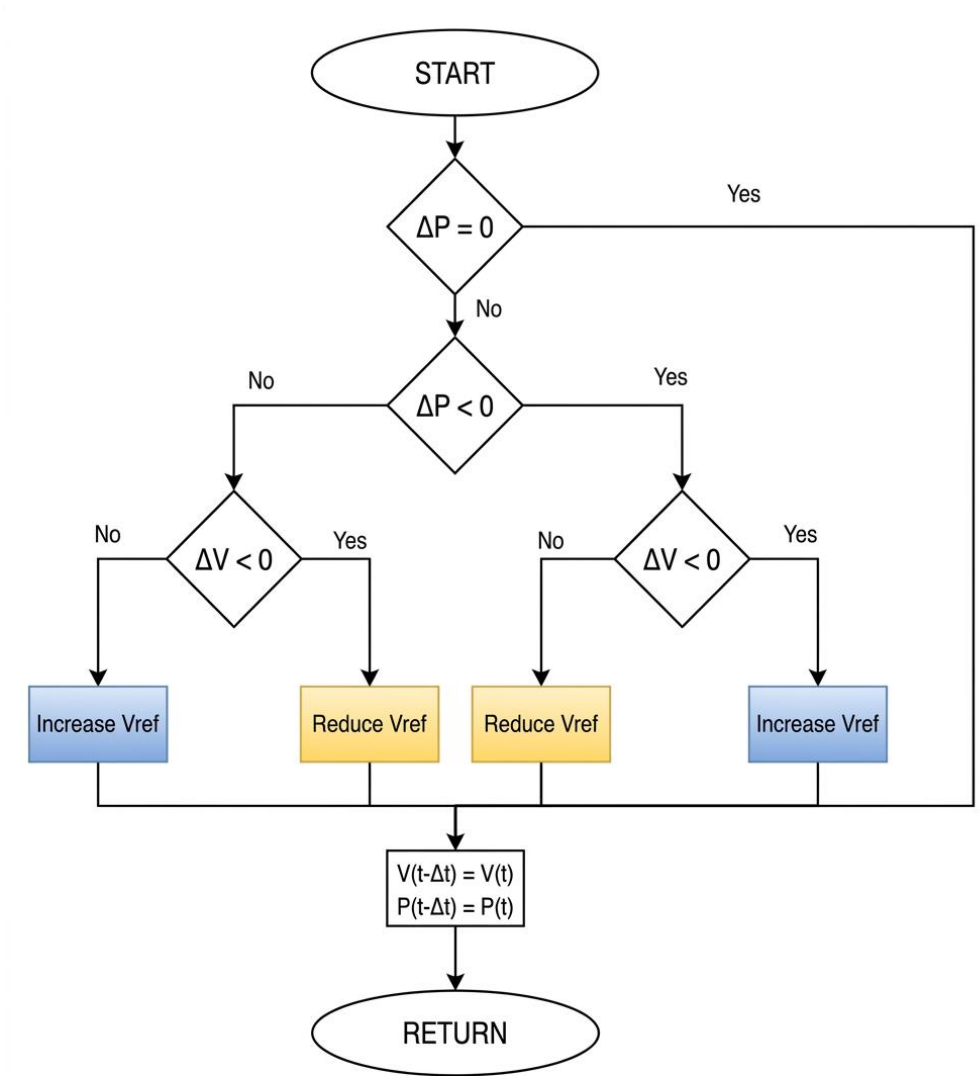

Figure 7: Flow chart of the conductivity increase method [10].

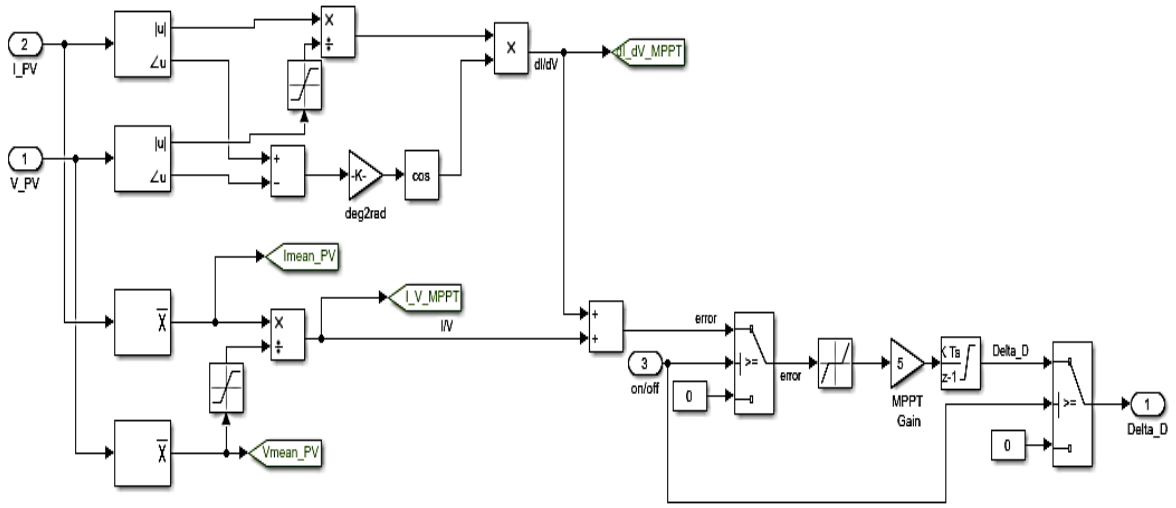

Figure 8: Modeling the conductivity increase method in Matlab.

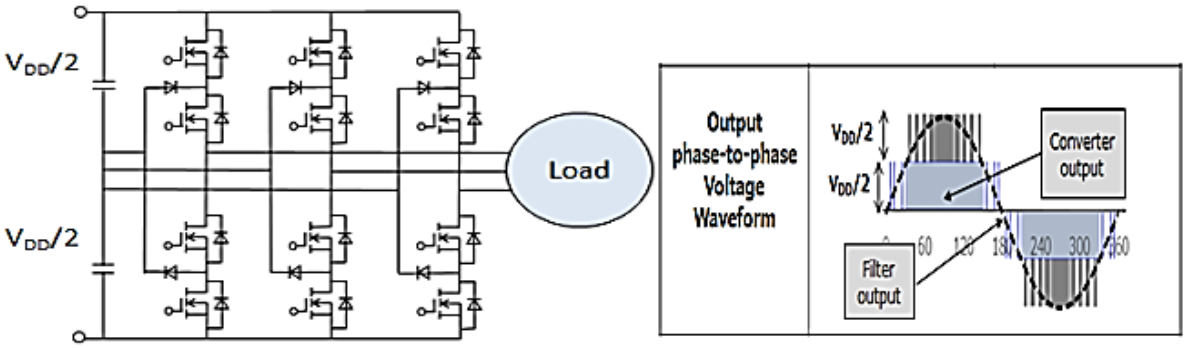

Figure 9: Three-phase inverter structure.

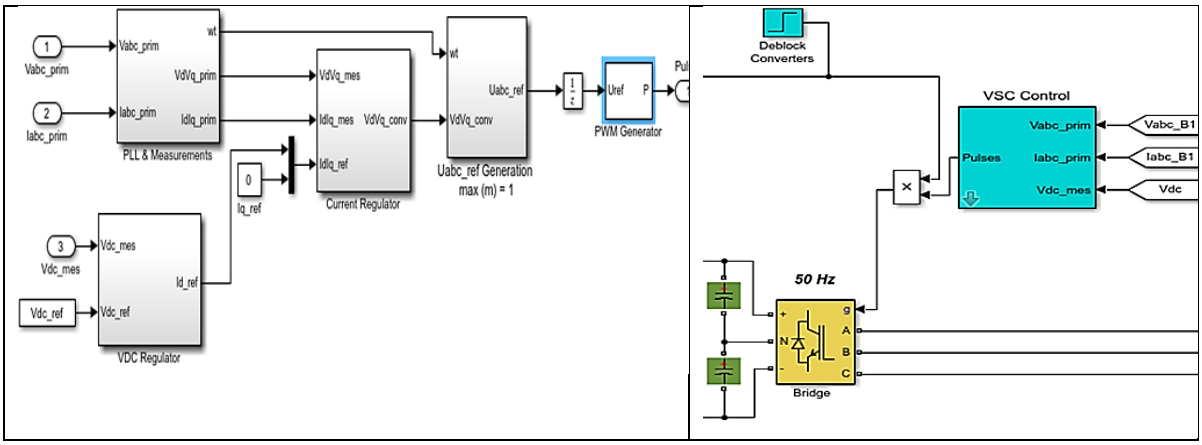

Figure 10: Modeling of a three-phase inverter driven by PWM technology.

2.4 Three-Phase Inverter

The DC input voltage of the inverter must be:

$$VDC > [\sqrt{2}\ V_g\ ]. \quad (5)$$

V_g: grid voltage.

$$VDC > (\sqrt{2} \times 220) > 311 = 400\ [V]$$

The three-phase three-level bridge as shown in Figure 9 is a bridge consisting of three arms, each arm having four IGBT elements, two upper and two lowers [17]:

The three-phase inverter-driven PWM is modeled as shown in Figure 10.

2.5 Passive Filters

A three-phase transmission line, which functions as an inductor, is utilized to transfer the maximum power from the photovoltaic panels to the public grid [18]. The inductance is calculated using following:

$$L = \frac{E^2}{2\pi F \times P_{max}}. \quad (6)$$

E: line voltage of grid [KV]. P max: maximum power transmitted by three phases [MW]. F: grid frequency [HZ].

Considering: P_{max} =10[KW] = 0.01[MW]، F =50[HZ]، E= 380[V] =0.38[KV].

The value of inductance for each phase is:

$$L = 0.38^2 / (2\pi \times 50 \times 0.01) = 0.046[H] = 46[mH]$$

This inductor also acts as a passive filter for current, then photovoltaic system is connected to a transformer center that raises the voltage from 380[V] to 20[KV] and then to public grid 20[KV].

3 HYBRID ENERGY STORAGE SYSTEM (HESS)

The maximum energy required to be provided by the hybrid storage system must be known, as calculated from [5], [19]:

$$E_{max} = \frac{P_{PV,nom}}{3600 \times T_m}. \quad (7)$$

- $P_{PV,nom}$: Nominal power generated by the cells [KW];
- T_m: Power management time [S].

Assuming that: $P_{PV,nom}$= 10 [KW], Tm=30[min]×60=1800[S]

We find: E max="10[KW]" /3600×1800 [S]=5 [KWh].

The percentage distribution of energy between batteries (E_b) and supercapacitors (E_{sc}) is calculated based on the ratio between the time constant of the battery response (τ), which is inversely proportional to the battery stress, and the energy management time Tm, batteries and supercapacitors energy is given as follows [11]:

$$E_b = \frac{1-\tau}{T_m} \times E_{max}, E_{sc} = \frac{\tau}{T_m} \times E_{max}, \quad (8)$$

We will design a hybrid storage system (comprising batteries and supercapacitors) following these steps:

1) Determine the parameters of the batteries (number, type, and specifications).
2) Determine the parameters of the supercapacitors (number and specifications).
3) Design a Buck/Boost converter for charging and discharging the batteries and supercapacitors

3.1 Battery Parameters

Lithium-ion batteries were selected due to their numerous advantages over other types, including higher efficiency and energy density (90%, 125 [Wh/kg]), increased nominal voltage (3.7 [V] per cell), lower weight, longer lifespan, faster and more efficient charging, smaller size, no maintenance requirements, and greater resistance to external conditions [11], [20].

Therefore, we select a GTK Lithium-ion battery C-2440H, with the following specifications [21]:

U_b = 24 [V], Cb = 30 [Ah] : τ=2.4 [min]

And considering: T_m = 30[min], and by compensating for (8) is:

$$E_b = 4.6\ [KWh]$$

To determine the number of batteries needed, we follow these steps:

1) Determine the required voltage of the battery matrix:

$$U_{b-total} = 200\ [V].$$

2) Determine the amount of energy required from the batteries:

$$E_b = 4.6/0.7 \approx 6\ [KWh].$$

Note: Since lithium-ion batteries operate in the capacity range of 25-95%, for safe use, only 70% of the theoretical energy is available [10][22]. Therefore, the calculated value of the total energy that

the battery should provide should be divided by 0.7 to obtain the correct values.

3) Calculate the total capacity of the batteries:

$$C_b = \frac{E_b}{U_{b-total}} = 30\ [\text{Ah}]. \quad (9)$$

4) Calculate the number of batteries in series:

$$N_S = \frac{U_{b-total}}{U_b} = 200/24 \approx 8. \quad (10)$$

5) Calculate the number of parallel strings:

$$N_B = \frac{C_{b-total}}{C_b} = \frac{30}{30} = 1. \quad (11)$$

6) Calculate the total number of batteries:

$$N = N_s \times N_b = 8. \quad (12)$$

3.2 Supercapacitors Parameters

From (8) in the previous section, we determined that the energy required from supercapacitors is:

$$E_{sc} = \frac{\tau}{T_m} \times E_{max} = 0.4\ [\text{kWh}].$$

To determine the specifications and number of capacitors, we select a supercapacitor from Maxwell Company, model BMOD0165 P048 C01with the following specifications [23]: U_{sc}=48 [V], C_{sc}=165 [F].

To determine the number of supercapacitors required, we follow these steps:

1) Determine the required capacitor array voltage:

$$U_{sc-total} = 200\ [\text{V}]$$

2) Determine the amount of energy required from the supercapacitor:

$$E_{sc} = 0.4\ [\text{KW}h].$$

Note: The supercapacitor module is typically designed to operate between the nominal voltage of the module $U_{scmax} = U_{scn}$ and half of its nominal voltage $U_{scmin} = \frac{U_{scn}}{2}$, Hence [2], [24]:

$$E_{sc} = \frac{3}{4}\left(\frac{1}{2} \times C_{sc-total} \times U_{sc-total}^2\right). \quad (13)$$

3) Calculate the total capacitance of the supercapacitor:

$$C_{sc-total} = \frac{E_{sc}}{0.75 \times 0.5 \times U_{sc-total}^2} = \frac{0.4 \times 1000 \times 3600}{0.75 \times 0.5 \times 200^2} = 96[F]. \quad (14)$$

4) Calculate the number of supercapacitors in series:

$$N_s = \frac{U_{sc-total}}{U_{sc}} = \frac{200}{48} \approx 4. \quad (15)$$

5) Calculate the total capacitance of the series:

$$C_s = \frac{C_{sc}}{N_s} = \frac{165}{4} = 41[F]. \quad (16)$$

6) Calculate the number of parallel strings:

$$N_b = \frac{C_{sc-total}}{C_s} = \frac{96}{41} = 2. \quad (17)$$

7) Calculate the total number of supercapacitors:

$$N = N_s \times N_b = 8. \quad (18)$$

3.3 Buck/Boost Converter

Figure 11 shows the structure of buck/boost converter.

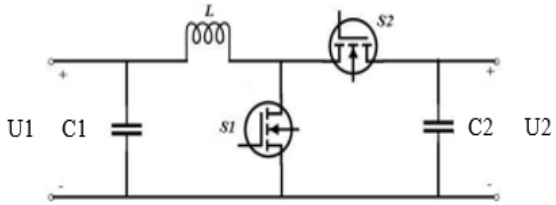

Figure 11: Buck/boost converter component [12].

The converter is designed taking into account the following requirements.

Output power (output power of the branch section at voltage 400 [V] where the output current of the array is 47.5 [A]) P_o =19000[w], Input voltage: U_1 = 200 [V], Output voltage: U_2 = 400 [V].

Chopping frequency F_s = 20000 [HZ], $\Delta U \leq 1$ [%]

Therefore, the maximum current of the IGBT is:

$$I_s = \frac{P_o}{U_1} = 95[A]. \quad (19)$$

If we consider the tolerance to be twice as large to get the maximum power from the storage source [12], [25], we find: $2 \times I_s$ = 190 [A].

The maximum voltage of IGBT is: IGBT V_{max} = U_2= 400 [V]. Considering the overload, the high voltage resulting from switching, and other factors, the maximum voltage of the IGBT should be greater than 400 [V].

As for the duty cycle factor, there are two factors:

The first is when the converter is in the boost position, which is:

$$D_1 = \frac{1-U_1}{U_2} = \frac{1-200}{400} = 0.5. \quad (20)$$

The second is when converter is working in buck mode, which is:

$$D_2 = \frac{U_1}{U_2} = \frac{200}{400} = 0.5. \quad (21)$$

The value of the inductor is calculated based on the following:

$$L = \frac{U_1 \times D_1}{\Delta I \times F_S}. \quad (22)$$

But according to engineering experience, half the current through the inductor is chosen to be 30% of the current Is. This enables us to obtain the minimum value of the inductor [26], [29], so it is:

$$\frac{\Delta I}{2} = 0.3\, I_s \;\rightarrow\; \Delta I = 0.6 \times I_s = 57. \quad (23)$$

By substitution in (22), L is:

$$L = \frac{200 \times 0.5}{57 \times 20000} = 88 \times 10^{-6}[H]. \quad (24)$$

For modeling L = 100 [mH].

As for the capacitance C_1, it is calculated in the reduced position according to:

$$C_1 = \frac{U_2 \times D_2 (1 - D_2)}{8 \times F_S^2 \times L \times \Delta U}. \quad (25)$$

Substituting the design requirements, we find:

$$C_1 = \frac{400 \times 0.5(1-0.5)}{8 \times 20000^2 \times 100 \times 10^6 \times 0.01} = 0.03 \text{ [F]}. \quad (26)$$

As for the capacity C2, it is calculated in boost position according to:

$$C_2 = \frac{I_O \times D_1}{F_S \times \Delta U}. \quad (27)$$

And it is:

$$I_o = \frac{P_o}{U_2} = \frac{19000}{400} = 47.5[A]. \quad (28)$$

$$C_2 = \frac{47.5 \times 0.5}{20000 \times 0.01} = 0.12[F]. \quad (29)$$

3.4 Control of Buck/Boost Converter and Energy Management

The control is implemented using a voltage and current double closed-loop as the primary controller, as illustrated in Figure 12.

The control system comprises an external voltage loop and an internal current loop. The external voltage loop is obtained by comparing V_b with V_{ref}, and the difference signal is sent to the PI controller. The resulting signal then enters the current loop, where it is compared with Ib, and the difference signal is sent to the PI controller and subsequently to the PWM system. This configuration ensures stable voltage on the U_2 side and current on the U1 side [5], [27], [30].

For system energy management, the flow chart shown in Figure 13 was adopted.

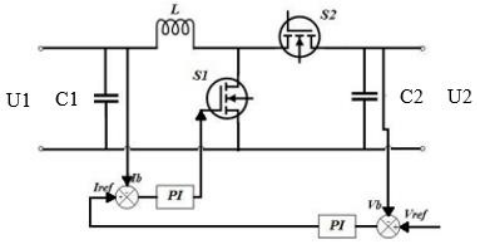

Figure 12: Control of bidirectional buck/boost converter [12].

4 MODELING OF THE PROPOSED SYSTEM AND RESULTS

Figure 14 shows modeling of the proposed system as a whole.

After operating the circuit shown in Figure 15, we obtained the following results:

4.1 Power

The energy stored in the batteries and capacitors will be utilized when the output power of the solar cells decreases. This occurs during the periods when the load obtains its energy from the grid, as shown in Figure 15, so power management time is: T_m=30[S]. Figure 16 shows us the (power-time) curve for each of the photovoltaic array power Ppv, the grid power Pg, the load power P_l, the batteries power P_{ba}, and the supercapacitor power P_{sc}.

We note that batteries acted as a high energy density storage element to meet the low frequency power requirements, and were discharged when the PV system output power decreased ($P_l > P_{pv}$) during the time periods (0-0.75), in order to cover the load requirements, when P_{pv} = 0 during the periods (0-0.57), the batteries discharged their energy to the load and the grid, and when the PV system started to produce power during the periods (0.57-0.75), the load was fed from the PV system and the batteries together (the batteries were discharged to the minimum charge state), and the excess power was injected into the grid, and at the minimum charge state at time 0.75, batteries stopped discharging and the load was fed from the PV system, after which it became ($P_l < P_{pv}$) during the time periods (0.75-1.7), and then the PV system started to charge batteries and feed the load in addition to injecting The excess power in the grid until the batteries were fully charged

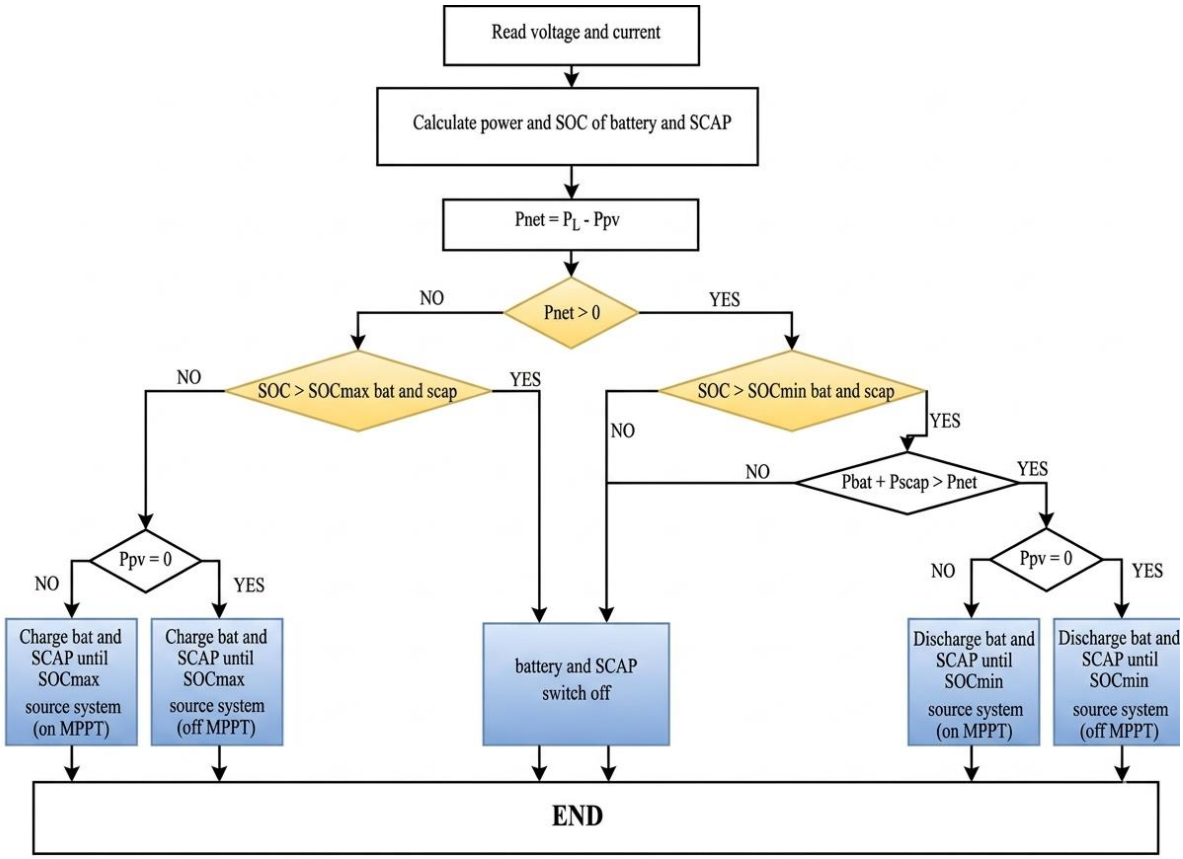

Figure 13: Flow chart for system energy management.

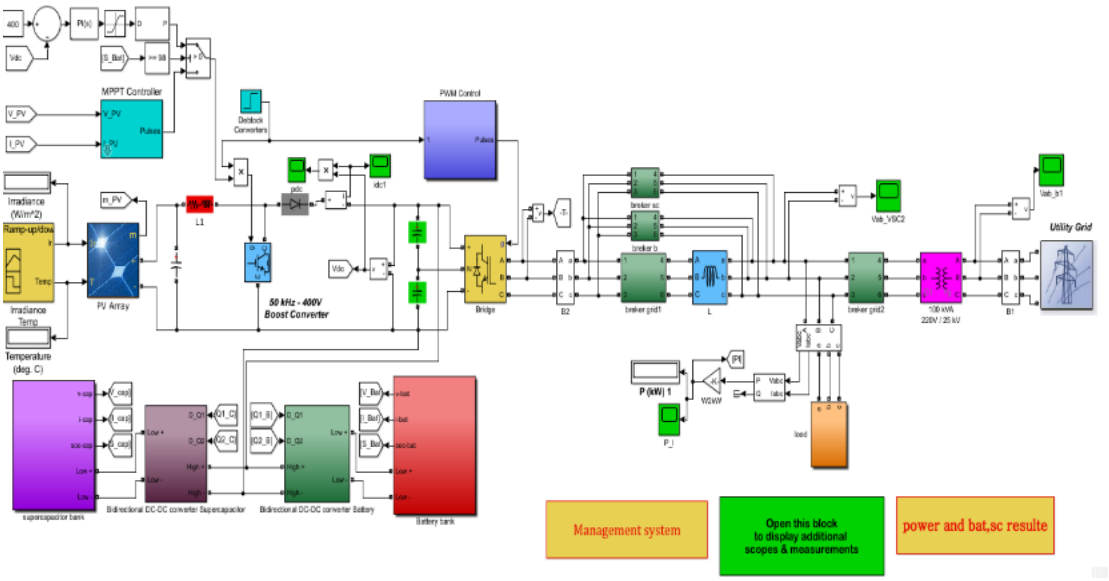

Figure 14: Modeling of the proposed system.

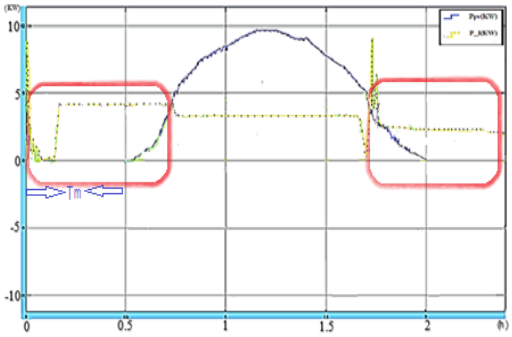

Figure 15: The periods during which the load obtains energy from the grid.

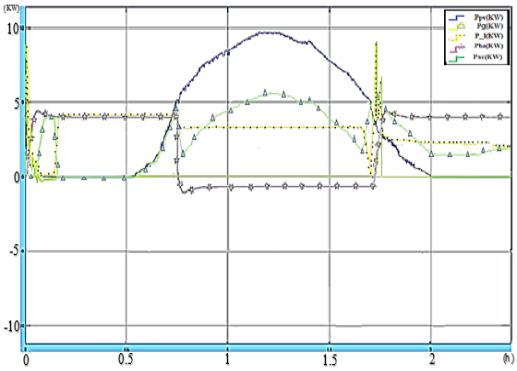

Figure 16: The power-time curve: P_{pv}, P_g, P_l, P_{ba}, P_{sc}.

(maximum charge state) at time 1.7, then the system continued to feed the load and the remaining power was injected into the grid, then a new battery discharge phase began. The supercapacitors acted as a high-energy density storage element to respond to high-frequency power requirements (transient load periods), as they were charged and discharged during these periods (0-0.04, 1.75-1.79).

As a result, when comparing Figure 16 and Figure 17, we notice that the batteries and supercapacitors work to cover the load requirements when the PV system power decreases, and thus reduce the draw from the grid (injecting excess power) while improving its stability.

4.2 Batteries Parameters

Figure 17 shows us the changes in the battery voltage v-bat, its current I-bat, its state of charge S-bat, and its capacity pbat concerning time:

From Figure 17, we observe that the batteries were discharged (the state of charge dropped from 80% to a minimum of 20%) when the photovoltaic system was unable to meet the load requirements. The output voltage of the batteries dropped to approximately 200 [V], the discharge current was about 23 [A], and the discharged power was 4.5 [kW]. Subsequently, the charging phase began (the state of charge rose from 20% to nearly 90%). The output voltage of the batteries was around 230 [V], the charging current was about 5 [A], and the charged power was 1.15 [kW].

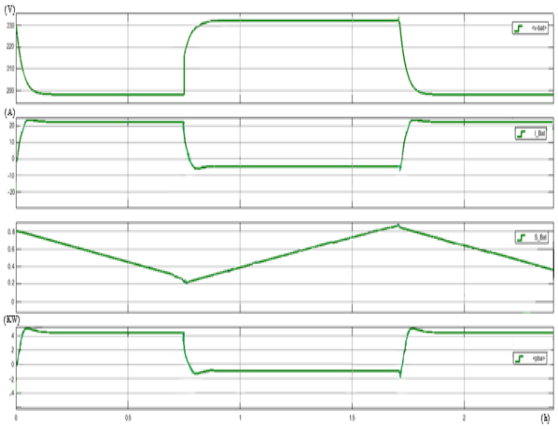

Figure 17: Changes in v-bat, I-bat, S-bat, pbat with Respect to Time.

4.3 Supercapacitors Parameters

Figure 18 illustrates the changes in the voltage of the capacitors V_{cap}, their current I_{cap}, their state of charge S_{cap}, and their capacity psc with respect to time:

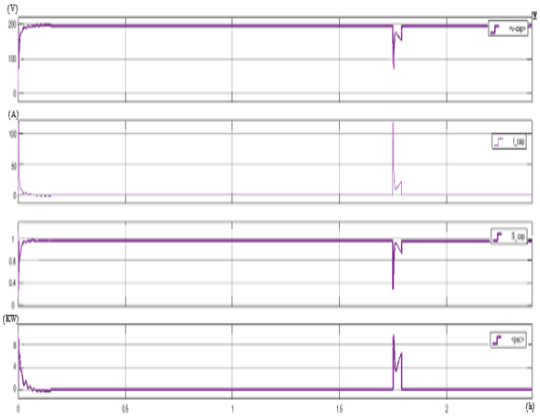

Figure 18: Variations of V_{cap}, I_{cap}, S_{cap}, P_{sc} with respect to time.

Figure 18 shows that the supercapacitors were charged and discharged with variable voltage and current to respond to high-frequency power requirements (transient load periods), thereby relieving the stress on the battery and stabilizing the public grid.

5 CONCLUSIONS

10 [kW] photovoltaic system was designed and modeled, demonstrating its ability to connect to the public grid regardless of changes in the input voltage of the panels, where the method of increasing conductivity were used to raise and regulate the output voltage of the cells to 400 [V] and to operate at the maximum power point.

The design and modeling of a three-phase voltage regulator driven by PWM technology resulted in an output voltage of 220 [V] for the alternating phase and 380 [V] for the line voltage, suitable for connection to the public grid.

A hybrid energy storage system consisting of batteries, supercapacitors, and a buck/boost converter was designed for charging and discharging, controlling their operation, and managing system power. The batteries acted as high-energy density storage elements to meet low-frequency power requirements, while the supercapacitors acted as high-power density storage elements to respond to high-frequency power requirements (transient periods). Both were discharged when the PV system output power decreased. Consequently, the power draw from the grid was reduced, and in some cases, the excess power was injected into the grid (which could be sold), thereby improving power quality and stability.

The energy required for both batteries and supercapacitors were calculated. It was found that considering a power management time of 30 minutes and a total stored energy of 5 [kWh], the ratio $\tau / T_m = 8[\%]$ is a good indicator that supercapacitors support the batteries for more than 2 minutes (30×8%=2.4), confirming that the supercapacitors have relieved the stress on the batteries, leading to an increased lifespan compared to an energy storage system that relies solely on batteries.

ABBREVIATIONS

MPPT	Maximum power point tracking
BDC	Bidirectional DC-DC converters
PWM	Pulse width modulation
ESS	Energy Storage Systems
BESS	Battary Energy Storage Systems
PI	Proportional-Integral
HESS	Hybrid Energy Storage System
Eb	Energy of batteries
Esc	Energy of supercapacitors

REFERENCES

[1] Yuldoshev, S. Shoguchkarov, T. Jamolov, and Sh. Rustamova, “Features of operation of the grid connected photovoltaic power station with a capacity of 10 kW,” E3S Web of Conferences, vol. 216, pp. 1–8, Dec. 2020, doi: 10.1051/e3sconf/202021601172.

[2] Yuldoshev, Y. Kurbanov, Sh. Rustamova, et al., “Modeling the operation of a 10 kW grid-tied photovoltaic power plant and its features,” AIP Conference Proceedings, vol. 2552, pp. 1–7, Jan. 2022, doi: 10.1063/5.0113931.

[3] D. Borkowski, P. Oramus, and M. Brzezinka, “Battery energy storage system for grid-connected photovoltaic farm – Energy management strategy and sizing optimization algorithm,” Journal of Energy Storage, vol. 72, part A, 2023, doi: 10.1016/j.est.2023.108201.

[4] Gonçalves, G. Cavalcanti, and M. Feitosa, “Optimal sizing of a photovoltaic/battery energy storage system to supply electric substation auxiliary systems under contingency,” Energies, vol. 16, 2023, doi: 10.3390/en16135165.

[5] M. Ongaro and P. Mattavelli, “Li-ion battery–supercapacitor hybrid storage system for a long lifetime photovoltaic-based wireless sensor network,” IEEE Transactions on Power Electronics, vol. 27, no. 9, 2021, doi: 10.1109/TPEL.2012.2189022.

[6] M. Kurtoğlu and F. Eroğl, “Design and simulation of bidirectional DC-DC converter topology for battery applications,” E3S Web of Conferences, vol. 551, 03002, 2024, doi: 10.1051/e3sconf/202455103002.

[7] V. Manuel, M. Ángel Guerrero, and F. Barrero, “A grid connected photovoltaic inverter with battery–supercapacitor hybrid energy storage,” Sensors, vol. 18, 2017.

[8] R. Rajasekaran and P. Usha Rani, “Energy management control algorithm based bidirectional DC-DC converter for small scale micro grid with hybrid storage system,” 2019, doi: 10.35940/ijeat.F1008.0886S19.

[9] Y. Jiao, Hybrid energy storage systems: Capacity optimization and environmental implication of hybrid energy storage systems in renewable power systems, Ph.D. dissertation, Stockholm, Sweden, 2022.

[10] K. Saritha et al., “Green energy storage solutions: A research,” E3S Web of Conferences, vol. 552, 01129, 2024, doi: 10.1051/e3sconf/202455201129.

[11] D. Abbes, F. Bensmaine, and A. Labrunie, “Energy management and batteries lifespan estimation in a photovoltaic system with hybrid storage: A comparative study,” IEEE, 2016.

[12] M. Nazeri and N. Abd Rahman, “Maximum power point tracking using perturb and observe technique,” Journal of Engineering Technology, vol. 10, no. 1, pp. 204–210, 2022. [Online]. Available: https://bmi.unikl.edu.my/wp-content/uploads/2022/11/204_210_Maximum-Power-Point-Tracking-Using-Perturb-and-Observe-Technique.pdf.

[13] Baboselac, Ž. Hederić, and T. Benšić, "Matlab simulation model for dynamic mode of lithium-ion batteries to power the EV," Technical Journal, vol. 11, no. 1–2, pp. 7–13, 2019. [Online]. Available: https://www.researchgate.net/publication/319355500_MatLab_simulation_model_for_dynamic_mode_of_the_Lithium-Ion_batteries_to_power_the_EV.

[14] Yustikasari, A. Azizah, E. Sunarno, and P. Putra, "Design and simulation of buck converter with fuzzy logic control for battery charging," Jurnal Ecotipe, vol. 8, pp. 59–64, 2021, doi: 10.33019/jurnalecotipe.v8i2.2389.

[15] K. Mongrid, V. Viswanathan, and J. Alam, Energy storage technology and cost characterization report, U.S. Department of Energy, Jul. 2019. [Online]. Available: https://www.pnnl.gov/publications/energy-storage-technology-and-cost-characterization-report.

[16] R. Rajasekaran and P. Usha Rani, "Energy management control algorithm based bidirectional DC-DC converter for small scale micro grid with hybrid storage system," International Journal of Engineering and Advanced Technology, vol. 8, no. 6S, 2019. [Online]. Available: https://www.ijeat.org/wp-content/uploads/papers/v8i6S/F10080886S19.pdf.

[17] T. A. Aika and F. O. Agbontaen, "Design and simulation of a DC–DC boost converter," 2023. [Online]. Available: https://www.researchgate.net/publication/369913957_DESIGN_AND_SIMULATION_OF_A_DC_-DC_BOOST_CONVERTER.

[18] N. V. Uma Maheswari and L. J. Shanthi, "Implementation of modified incremental conductance MPPT algorithm in grid connected PV system under dynamic climatic conditions," Indian Journal of Science and Technology, vol. 15, no. 17, pp. 819–828, 2022, doi: 10.17485/IJST/v15i17.282.

[19] M. Hammami, R. Mandrioli, and G. Grandi, "Capacitor voltage switching ripple in three-phase three-level neutral point clamped inverters with sinusoidal carrier-based PWM," 2018, doi: 10.1109/INDEL.2018.8637643.

[20] M. Saleem, M. H. A. K. Khushik, and H. Tahir, "Robust L approximation of an LCL filter type grid-connected inverter using active disturbance rejection control under grid impedance uncertainty," Energies, vol. 14, p. 5276, 2021, doi: 10.3390/en14175276.

[21] H. V. Nguyen et al., "Enhancing effectiveness of grid-connected photovoltaic systems by using hybrid energy storage systems," Journal of Engineering Science and Technology, vol. 16, no. 2, pp. 1561–1576, 2021. [Online]. Available: https://jestec.taylors.edu.my/Vol%2016%20issue%202%20April%202021/16_2_47.pdf.

[22] Ch. Hermanu et al., "Optimal planning of battery energy storage systems by considering battery degradation due to ambient temperature: A review, challenges, and new perspective," Batteries, vol. 8, p. 290, 2022, doi: 10.3390/batteries8120290.

[23] Maxwell Technologies, "48V module datasheet: BMOD0165 P048 C01," 2021. [Online]. Available: https://maxwell.com/wp-content/uploads/2021/08/48V_ds_DuraBlue_3000685_4.pdf.

[24] Y. Wang et al., "Fast charging of energy-dense lithium-ion batteries," Nature, vol. 611, pp. 485–490, 2022.

[25] P. Resutík, S. Kaščák, and M. Praženica, "Design of a supercapacitor module and control algorithm for practical verification of a hybrid energy storage system," Applied Sciences, vol. 14, p. 1035, 2024, doi: 10.3390/app142210357.

[26] S. A. Aviles, A. H. Kadam, T. Sidhu, and S. S. Williamson, "Modeling, analysis, design, and simulation of a bidirectional DC-DC converter with integrated snow removal functionality for solar PV electric vehicle charger applications," Energies, vol. 15, p. 2961, 2022, doi: 10.3390/en15082961.

[27] K. K. Pandey et al., "Bidirectional DC-DC buck-boost converter for battery energy storage system and PV panel," 2022, doi: 10.1007/978-981-15-9829-6_54.

[28] V. Viswanatha, V. S. Reddy, and R. Rajeswari, "Closed loop control of bidirectional buck-boost converter for battery management in automotive systems," International Journal of Advance Science and Technology, vol. 29, no. 10S, pp. 8568–8580, 2020.

[29] E. Atawi et al., "Recent advances in hybrid energy storage system integrated renewable power generation: Configuration, control, applications, and future directions," Batteries, vol. 9, p. 29, 2023, doi: 10.3390/batteries9010029.

[30] M. Kurtoğlu and F. Eroğl, "Design and simulation of bidirectional DC-DC converter topology for battery applications," E3S Web of Conferences, vol. 551, 03002, 2024, doi: 10.1051/e3sconf/202455103002.